

Effects of texture on lattice constants of Nd₂Fe₁₄B and their relationship with internal stress in Nd-Fe-B permanent magnets

S. Kobayashi^{1,2}, A. Martín-Cid^{1,2}, K. Toyoki^{1,2,*}, H. Okazaki^{1,2,†}, S. Kawaguchi¹, S. Hirose², and T. Nakamura^{1,2}

¹Japan Synchrotron Radiation Research Institute (JASRI), 1-1-1 Kouto, Sayo 679-5198, Japan

²Elements Strategy Initiative Center for Magnetic Materials (ESICMM), National Institute for Materials Science, Tsukuba 305-0047, Japan



(Received 2 May 2020; accepted 17 August 2020; published 14 September 2020)

Although crystallographic properties are considered to be intrinsic, several studies have reported significant different values for the lattice constants of the Nd₂Fe₁₄B phase. In this study, by analyzing rod-shaped isotropic (randomly oriented) and anisotropic (*c*-axis oriented) Nd-Fe-B bulk-sintered magnets, their powdered counterparts, and powder made from grinding a single crystal, we experimentally demonstrate that the lattice constants of the Nd₂Fe₁₄B phase in the ferromagnetic ordering state depend on the sample texture. The temperature dependence of the lattice constants was investigated by focusing on their expansion associated with ferromagnetic ordering, that is, the spontaneous linear expansion along the *a*-axis (λ_a) and *c*-axis (λ_c). The λ_a value of the isotropic (anisotropic) bulk-sintered magnets at 105 K is 10% (2%) smaller while the λ_c value is 130% (40%) greater than that of the powdered single crystal. These results indicate the presence of an internal stress perpendicular to the *c*-axis in the isotropic and anisotropic bulk-sintered magnets. In addition, we observed that the ratios of the length along the *a*-axis to that along the *c*-axis (*c/a*) for the various Nd-Fe-B magnets as well as those reported previously are correlated to the sample texture. In other words, the *c/a* values of the sintered magnets are greater than those of the powdered samples. This result suggests that the sample texture and hence the internal stress has a determining effect on the lattice constants.

DOI: [10.1103/PhysRevMaterials.4.094405](https://doi.org/10.1103/PhysRevMaterials.4.094405)

I. INTRODUCTION

The Nd₂Fe₁₄B compound is used in permanent magnets for many applications, such as hard disk drives, cell phones, the traction motors of electric vehicles, and wind turbines. This is because of its outstanding magnetic properties, namely, its high Curie temperature, T_C , of ≈ 585 K, large magnetization of 1.6 T, and large anisotropy field of 7.3 T at 300 K [1–6]. Since its discovery to date, the compound's intrinsic properties have been thoroughly investigated, and these types of magnets are being reinvestigated, even recently, due to strong demand for the ability to develop permanent magnets without relying on the geopolitically critical elements Dy and Tb [4–11]. However, the accumulated information in the literature contains discrepancies that can potentially create confusion. The discrepancy in lattice constants is a typical example. Although the lattice constants of a material are considered to be its intrinsic characteristics, those of the Nd₂Fe₁₄B phase show significant variations, even at the same temperature, as per the results of several studies. For instance, its previously reported *a* and *c* values at room temperature range from 8.79 to 8.81 Å and from 12.17 to 12.23 Å, respectively [12–39] (see Table S1 of the Supplemental Material

[40]). These variations suggest the existence of a secondary factor that also affects the lattice constants. The lattice constants are often used as an index to quantify the extent of elemental substitution [26,41,42]. However, the existence of this secondary factor could reduce their accuracy in this regard significantly. Moreover, it would also affect the reliability and efficiency of theoretical calculations. Therefore, elucidating the factor that causes these variations in the lattice constants would enhance our understanding and promote further development of Nd-Fe-B magnets.

Several factors can induce variations in the lattice constants, including small differences in the chemical composition as well as experimental errors. Given the large spontaneous volume magnetostriction of the Nd₂Fe₁₄B phase, which is highly anisotropic [27,30,43–48], even slight changes in the spontaneous magnetostrictive behavior are expected to have a significant effect on the lattice constants at temperatures lower than T_C . Whereas some magnets exhibit a change in their shape (magnetostriction) during magnetization using an external magnetic field, the ferromagnetic alloys called invar alloys exhibit volume expansion (spontaneous magnetostriction), which is associated with ferromagnetic ordering even in the absence of an external magnetic field [49–52]. This change is induced by internal magnetization. Spontaneous magnetostriction should be a material-specific property. However, previous studies have reported contradictory results with respect to the spontaneous magnetostrictive behavior of the Nd₂Fe₁₄B phase. For example, using x-ray diffraction (XRD) analysis, Andreev *et al.* found that the linear expansion along the *a*-axis (λ_a) of single-crystalline Nd₂Fe₁₄B is

*Present address: Department of Materials Science and Engineering, Graduate School of Engineering, Osaka University, 2-1, Yamadaoka, Suita, Osaka 565-0871, Japan.

†Present address: National Institutes for Quantum and Radiological Science and Technology, 1233 Watanuki, Takasaki 370-1292, Japan.

approximately 4.5 times greater than that along the c -axis (λ_c) [30]. In contrast, Yang *et al.*, who studied spontaneous volume magnetostriction in the melt-spun ribbons of powdered $\text{Nd}_2\text{Fe}_{14}\text{B}$ using synchrotron XRD analysis, found that λ_a is only 1.8 times larger than λ_c [27]. The spontaneous volume expansion (ω_s) values of the material were similar at 2.0–2.3%, although the same values measured via dilatometry were slightly higher (2.4–2.8%) [43,46,47]. These results suggest that it is the differences in the spontaneous magnetostriction that cause the variations in the lattice constants of the $\text{Nd}_2\text{Fe}_{14}\text{B}$ phase at temperatures lower than T_C . However, owing to the numerous reasons for variation in the material lattice constants and their distribution in materials, such as grain size, interface stress, and internal stress, a systematic study using well-defined specimens is required.

Therefore, in this study, we performed synchrotron XRD analyses to investigate the temperature dependence of the lattice constants and spontaneous magnetostriction of the $\text{Nd}_2\text{Fe}_{14}\text{B}$ phase using different types of specimens. We used five samples with different but well-defined textures: isotropic (randomly oriented) and anisotropic (c -axis oriented) Nd-Fe-B bulk-sintered magnets, their powdered counterparts, and a powdered single crystal. Synchrotron XRD analysis has the advantage of allowing precise measurements of the lattice constants of constituent phases in both bulk and powder forms, owing to the high penetration and resolution of the high-energy synchrotron x-rays. Thus, in this study, we could experimentally demonstrate that the lattice constants of the $\text{Nd}_2\text{Fe}_{14}\text{B}$ phase and their distribution below T_C depend on the sample texture. The internal stress generated in the bulk samples was investigated as the source of differences in the lattice constants.

II. EXPERIMENT

As stated above, rod-shaped isotropic and anisotropic Nd-Fe-B bulk-sintered magnets and a powdered $\text{Nd}_2\text{Fe}_{14}\text{B}$ single crystal were used in this study. In addition, isotropic and anisotropic Nd-Fe-B sintered magnets were also used in the powdered form. The Nd-Fe-B sintered magnets were prepared by the previously reported method [28,29,53], which involved strip casting, hydrogen decrepitating, jet milling, and compaction of powder (without an external magnetic field for the isotropic sample and in the presence of one for the anisotropic sample), and subsequent sintering at 1293 K. The samples were cooled at a rate higher than 20 K/min. The average crystal grain size is approximately 5 μm , as confirmed by scanning electron microscopy (SEM, Hitachi TM3030plus) (Fig. S1 of the Supplemental Material [40]). The chemical compositions of the specimens were determined using inductively coupled plasma analysis and an oxygen analyzer with a nondispersive infrared detector; it was $\text{Nd}_{13.7}\text{Fe}_{78.2}\text{B}_{5.9}\text{Cu}_{0.10}\text{Pr}_{0.05}\text{Tb}_{0.02}\text{Al}_{0.12}\text{O}_{1.9}\text{N}_{0.03}$ at. % for the isotropic sintered magnet and $\text{Nd}_{13.8}\text{Fe}_{78.5}\text{B}_{5.9}\text{Cu}_{0.10}\text{Pr}_{0.05}\text{Tb}_{0.02}\text{Al}_{0.12}\text{O}_{1.4}\text{N}_{0.03}$ for the anisotropic sintered magnet (note that Pr, Tb, and Al are impurities). It is worth noting that a small amount of Cu was intentionally added to the Nd-Fe-B sintered magnets to enhance their coercivity; however, the Cu did not exist in the $\text{Nd}_2\text{Fe}_{14}\text{B}$ phase but was essentially concentrated at the

interface between the $\text{Nd}_2\text{Fe}_{14}\text{B}$ phase and the grain-boundary phase [7,54]. The magnetic properties of anisotropic sintered magnets synthesized using the aforementioned procedure have already been investigated by Yasui *et al.* using vibrating sample magnetometer (VSM) with the external field up to 2.0 T along the magnetic easy axis [53]. The coercivity value of the anisotropic sintered magnets without annealing was 0.67 T [53]. The coercivity of the isotropic sintered magnets without annealing, measured using VSM, was 1.35 T. The higher coercivity for the isotropic sintered magnets is in agreement with previous reports [55,56], which mention that the coercivity increases as the crystalline orientation degree of $\text{Nd}_2\text{Fe}_{14}\text{B}$ grains decreases. The magnetization hysteresis loops measured along the three different directions of the isotropic sintered magnets were identical, indicating the random orientation of crystal grains.

For the synchrotron XRD measurements of the Nd-Fe-B sintered magnets, rectangular rod-shaped bulk samples with dimensions of approximately 0.2 mm \times 0.2 mm \times 5 mm were used. These specimens were cut from a large sintered block. Rods of the anisotropic sintered magnets were prepared so that the longitudinal direction was perpendicular to the c -axis, which is the magnetic easy axis. Powdered samples were prepared by crushing the isotropic and anisotropic sintered magnets in an Ar glovebox to prevent the oxidation of the constituent phases. The average powder particle size was determined using SEM to be approximately 4 μm (maximum diameter of approximately 10 μm and many small particles with less than 0.5 μm in diameter) (Fig. S1 [40]). The rod-shaped bulk samples and the powdered isotropic and anisotropic sintered magnets were sealed in quartz capillary tubes (internal diameter of 0.3 mm) in an Ar atmosphere. Further, a single crystal of $\text{Nd}_2\text{Fe}_{14}\text{B}$ was prepared using the floating zone method [57]. Powder made from grinding a single crystal was sealed in a quartz capillary tube (internal diameter of 0.2 mm) in an Ar atmosphere.

The synchrotron XRD profiles were obtained using a high-resolution one-dimensional solid-state detector (MYTHEN) at beamline BL02B2 of the SPring-8 facility ($\lambda = 0.4962$ or 0.4970 \AA) without using an external magnetic field [58]. The capillary tubes containing the samples were spun continuously during the measurements to ensure a homogeneous XRD intensity. High- and low-temperature measurements were performed using an N_2 gas flow system. The measurement range was 100–900 K for the sintered magnets, 100–700 K for the powdered sintered samples, and 105–900 K for the powdered single crystal. The diffraction patterns were collected using a step size of 0.006°. Rietveld refinements were performed using the software RIETAN-FP [59] to determine the volume fraction of the constituted phase. Le Bail refinements were conducted to determine the lattice constants. The peak broadening was evaluated by the full width at half maximum (FWHM) of the Bragg peaks using the pseudo-Voigt function.

III. RESULTS

A. Synchrotron XRD patterns at 300 K

Figure 1 shows the synchrotron XRD profiles of the isotropic and anisotropic Nd-Fe-B bulk-sintered magnets and

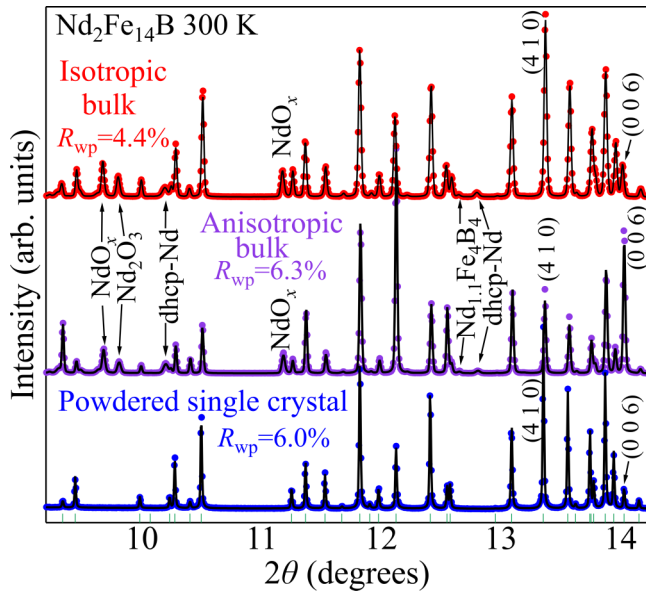


FIG. 1. Synchrotron x-ray diffraction patterns of isotropic and anisotropic Nd-Fe-B bulk-sintered magnets and powdered $\text{Nd}_2\text{Fe}_{14}\text{B}$ single crystal at 300 K (solid circles), along with the corresponding Le Bail refinements (solid curves). Numbers above profiles and green ticks represent indices and positions of reflections, respectively. Positions of diffraction peaks of dhcp-Nd, fcc- NdO_x , hcp- Nd_2O_3 , and $\text{Nd}_{1.1}\text{Fe}_4\text{B}_4$ are also shown. The weighed reliability factors, R_{wp} , obtained in the refinement are also shown.

the powdered $\text{Nd}_2\text{Fe}_{14}\text{B}$ single crystal at 300 K. The XRD pattern of the powdered single crystal was similar to that simulated using a previously reported structural model with the $P4_2/mnm$ space group [2]. The XRD profiles of the isotropic and anisotropic bulk-sintered magnets could be indexed to the $\text{Nd}_2\text{Fe}_{14}\text{B}$ phase and the following secondary phases: double hexagonal-close-packed Nd (dhcp-Nd) ($P6_3/mmc$) [60], face-centered-cubic NdO_x (fcc- NdO_x) ($Fm\bar{3}m$) [61], and hexagonal-closed-packed Nd_2O_3 (hcp- Nd_2O_3) ($P\bar{3}m1$) [62]. A few weak diffraction peaks related to the $\text{Nd}_{1.1}\text{Fe}_4\text{B}_4$ phase were also observed [63], although the precise volume fraction of this phase could not be determined from the subsequent Rietveld analysis owing to the low intensities of the peaks. The volume fractions of the constituent phases of the isotropic sintered magnet were determined from the Rietveld analysis and found to be 93.8% for $\text{Nd}_2\text{Fe}_{14}\text{B}$, 1.5% for dhcp-Nd, 2.7% for fcc- NdO_x , and 2.0% for hcp- Nd_2O_3 . In contrast to the isotropic sintered magnet, it was difficult to determine the precise volume fraction of the $\text{Nd}_2\text{Fe}_{14}\text{B}$ phase in the anisotropic sintered magnet due to the strong orientation of this phase. The FWHM of the rocking curve for the (0 0 2) diffraction peaks of the anisotropic sintered magnets was about 26° , indicating the preferred orientation. Using the orientation parameter along the [0 0 l] direction in the Rietveld analysis, however, the volume fractions of the constituent phases of the anisotropic sintered magnet could be estimated as 93.9% for $\text{Nd}_2\text{Fe}_{14}\text{B}$, 1.8% for dhcp-Nd, 2.7% for fcc- NdO_x , and 1.6% for hcp- Nd_2O_3 . The similar volume fractions of the $\text{Nd}_2\text{Fe}_{14}\text{B}$ phase in both magnets were as expected because of their similar chemical composition and the similar production

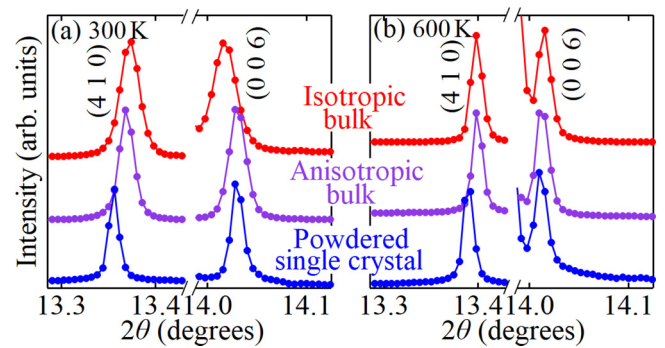


FIG. 2. Magnifications of the (4 1 0) and (0 0 6) peaks of $\text{Nd}_2\text{Fe}_{14}\text{B}$ phase in isotropic and anisotropic Nd-Fe-B bulk-sintered magnets and powdered single crystal at (a) 300 K and (b) 600 K.

process. The hcp- Nd_2O_3 and dhcp-Nd phases in the isotropic sintered magnets were slightly larger and smaller than those of the anisotropic ones, respectively, which is consistent with the larger oxygen content for the isotropic sintered magnet. Next, the lattice constants of the $\text{Nd}_2\text{Fe}_{14}\text{B}$ phase were determined through whole-pattern fitting using the Le Bail analysis method. This is the preferred technique for determining the lattice constants with precision when the variations in the peak intensities owing to the strongly preferred orientation reduce the accuracy of the Rietveld refinement method.

At 300 K, the isotropic and anisotropic bulk-sintered magnets and the powdered single crystal exhibited significant differences not only in the intensities of the diffraction peaks related to the $\text{Nd}_2\text{Fe}_{14}\text{B}$ phase, due to its preferred orientation, but also in the FWHM values of the peaks and their lattice constants. The FWHM values of the diffraction peaks of the isotropic and anisotropic bulk-sintered magnets at 300 K were larger than those of the powdered single crystal, as shown in Fig. 2(a). These results are discussed in greater detail in Sec. III C. The lattice constants of the $\text{Nd}_2\text{Fe}_{14}\text{B}$ phase of the three samples at 300 K were all different, as listed in Table I. The lattice constant a increased while the constant c decreased in the following order: isotropic bulk-sintered magnet, anisotropic bulk-sintered magnet, and powdered single crystal. The unit-cell volume V values of the isotropic and anisotropic bulk-sintered magnets were similar, while that of the powdered single crystal was slightly larger (0.1%) than those of the bulk-sintered magnets.

B. Temperature dependence of lattice constants

To elucidate the origin of the differences in the lattice constants of the $\text{Nd}_2\text{Fe}_{14}\text{B}$ phase in the various samples, we investigated the temperature dependence of the lattice constants in the samples (see Fig. 3). The determined lattice constant values are listed in Table I and in Table S2 of the Supplemental Material [40]. At temperatures higher than T_C , the values of a and c of the $\text{Nd}_2\text{Fe}_{14}\text{B}$ phase decreased monotonically with decreasing temperature for all the analyzed samples. Further, the c values of the samples at temperatures higher than T_C were similar, whereas the a value of the powdered single crystal was slightly larger than those of the isotropic and anisotropic bulk-sintered magnets.

TABLE I. Lattice constants (a and c), c/a ratio, and unit-cell volume (V) of isotropic and anisotropic Nd-Fe-B bulk-sintered magnets and powdered single crystal at 105, 300, and 600 K. Linear spontaneous magnetostriction values λ_a (along the a -axis) and λ_c (along the c -axis), and spontaneous volume magnetostriction (ω_s) at 105 and 300 K are also listed.

	Bulk-sintered magnets		Powdered single crystal
	Isotropic	Anisotropic	
	105 K		
a (Å)	8.798 89(4)	8.802 93(6)	8.810 34(5)
c (Å)	12.207 95(6)	12.193 03(8)	12.190 04(8)
c/a	1.387 44(1)	1.385 11(1)	1.383 61(1)
V (Å ³)	945.145(10)	944.855(12)	946.217(9)
λ_a	7.5×10^{-3}	8.1×10^{-3}	8.3×10^{-3}
λ_c	3.7×10^{-3}	2.2×10^{-3}	1.6×10^{-3}
ω_s	1.9×10^{-2}	1.8×10^{-2}	1.8×10^{-2}
	300 K		
a (Å)	8.800 03(3)	8.802 98(5)	8.809 93(5)
c (Å)	12.219 26(5)	12.208 99(6)	12.206 83(8)
c/a	1.388 55(1)	1.386 92(1)	1.385 57(1)
V (Å ³)	946.267(6)	946.098(9)	947.431(10)
λ_a	5.7×10^{-3}	6.2×10^{-3}	6.3×10^{-3}
λ_c	3.0×10^{-3}	2.0×10^{-3}	1.5×10^{-3}
ω_s	1.4×10^{-2}	1.4×10^{-2}	1.4×10^{-2}
	600 K		
a (Å)	8.782 90(3)	8.782 53(3)	8.787 55(5)
c (Å)	12.221 51(4)	12.223 44(4)	12.222 25(8)
c/a	1.391 51(1)	1.391 79(1)	1.390 85(1)
V (Å ³)	942.760(5)	942.830(6)	943.815(10)

In contrast, at temperatures lower than T_C , for all the samples, the lattice constants exhibited the typical temperature dependence seen in the case of invar-type alloys [49–52]. In other words, at temperatures lower than T_C , the lattice constants were higher than those extrapolated from the paramagnetic region, and the crystal symmetry was the same above and below T_C . Thus, the thermal expansion without magnetic contribution below T_C can be estimated from the extrapolation of the temperature dependence of the unit-cell volume in the paramagnetic region. The magnetic contribution to the unit-cell volume expansion can be estimated from the differences in the observed and extrapolated values of a , c , and V . The linear spontaneous magnetostrictive strain in the basal plane, λ_a , is $(a - a_0)/a_0$; that along the c -axis, λ_c , is $(c - c_0)/c_0$; and the spontaneous volume magnetostriction ω_s is $(V - V_0)/V_0$. Here, a_0 , c_0 , and V_0 represent the lengths along the a - and c -axis and the unit-cell volume, respectively, at temperatures lower than T_C , as extrapolated from the paramagnetic region. These values were calculated using a Debye approximation, for which the Debye temperature T_D was assumed to be 400 K based on previous reports [43,51]. The calculated values are exhibited in Table S3 [40]. At 105 K, the λ_a value of the Nd₂Fe₁₄B phase was several times larger than the λ_c value; this was true for all the samples (Table I). The above-described results are qualitatively similar to those reported previously [27,30,43–48]. However, while the change was observed in the lattice constants associated with the spin reorientation at

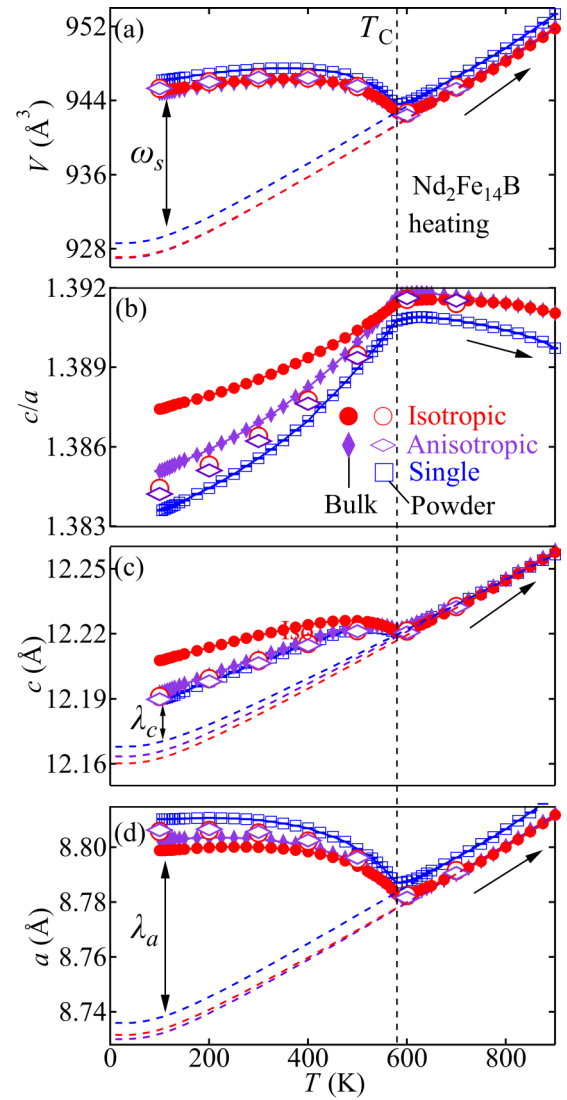


FIG. 3. Temperature dependence of lattice constants a and c , c/a ratio, and unit-cell volume V of Nd₂Fe₁₄B phase in isotropic (red circles) and anisotropic (purple diamonds) Nd-Fe-B bulk-sintered magnets, their powdered counterparts, and powdered Nd₂Fe₁₄B single crystal (blue squares). Solid and open symbols represent bulk-sintered magnets and powdered sample, respectively. The dashed lines, which correspond to a_0 , c_0 , and V_0 , represent the phonon contribution to the thermal expansion.

approximately 140 K in previous studies [27,30,43], it was too small to be observed over the investigated temperature range in the present study.

A remarkable trend was observed in the differences in the λ_a and λ_c values of the various samples, in that λ_a decreased while λ_c increased in the following order: powdered single crystal, anisotropic bulk-sintered magnet, and isotropic bulk-sintered magnet. Considering the similarity in the lattice constants of all three samples at temperatures above T_C , the differences in the lattice constants at temperatures below T_C can probably be attributed to the differences in the spontaneous magnetostrictive behaviors of the samples.

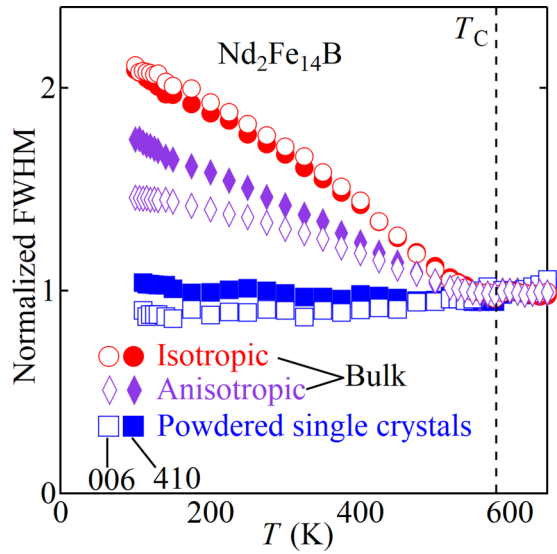


FIG. 4. Temperature dependence of the full width at half maximum (FWHM) of the (4 1 0) peak (solid markers) and (0 0 6) peak (open markers) of the $\text{Nd}_2\text{Fe}_{14}\text{B}$ phase in isotropic (red circles) and anisotropic (purple diamonds) bulk-sintered magnets and powdered single crystal (blue squares). The FWHMs are normalized by those at 600 K.

C. Broadening of diffraction peaks of bulk-sintered magnets below T_C

As described above, not only did the lattice constants of the samples vary at 300 K but so did the FWHM values of their diffraction peaks. In general, factors such as small particle size, nonuniform chemical composition, lattice defects, and lattice strain may cause peak broadening. To determine the origin of the broadening of the peaks of the $\text{Nd}_2\text{Fe}_{14}\text{B}$ phase for the isotropic and anisotropic bulk-sintered magnets, we investigated the temperature dependence of the FWHM values of the diffraction peaks of the $\text{Nd}_2\text{Fe}_{14}\text{B}$ phase.

Figure 2 compares the magnified versions of the (4 1 0) and (0 0 6) diffraction peaks of the $\text{Nd}_2\text{Fe}_{14}\text{B}$ phase of the various specimens corresponding to the ferromagnetic state at 300 K and the paramagnetic state at 600 K. The peak profiles and FWHM values of all three samples at 600 K are similar, indicating that the crystallinities of the $\text{Nd}_2\text{Fe}_{14}\text{B}$ grains in the three samples were also similar. At 300 K, the FWHM values of the diffraction peaks of the isotropic and anisotropic samples were greater than those of the powdered single crystal.

To determine the temperature at which the diffraction peaks begin to broaden, we investigated the temperature dependence of the FWHM values of the (4 1 0) and (0 0 6) peaks of the three samples (see Fig. 4). Here, the FWHM values were normalized with respect to those at 600 K to eliminate the effects of the dependence of the FWHM on the diffraction angle, 2θ [58]. Although the FWHM values of the (4 1 0) and (0 0 6) peaks of the powdered single crystal were almost temperature independent, those of the isotropic and anisotropic bulk-sintered magnets increased with the temperature for temperatures just below T_C . Thus, peak broadening in the cases of the isotropic and anisotropic

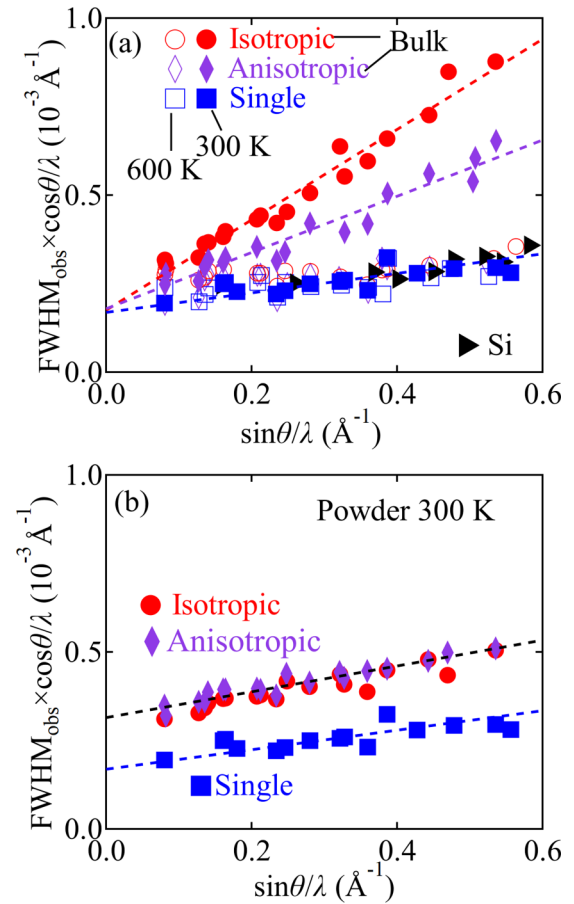


FIG. 5. (a) Williamson-Hall (WH) plots of the $\text{Nd}_2\text{Fe}_{14}\text{B}$ phase in isotropic and anisotropic bulk-sintered magnets and powdered single crystal at 600 K (open markers) and 300 K (solid markers), and a standard Si sample. (b) WH plots of the $\text{Nd}_2\text{Fe}_{14}\text{B}$ phase in powdered isotropic and anisotropic bulk-sintered magnets and powdered single crystal at 300 K. The dashed lines are included solely to aid reader comprehension.

bulk-sintered magnets began at temperatures below T_C , suggesting that the phenomenon is closely related to the magnetic ordering or spontaneous magnetostriction of the $\text{Nd}_2\text{Fe}_{14}\text{B}$ phase.

The phenomenon of peak broadening was investigated further by analyzing the 2θ dependence of the FWHM values using Williamson-Hall (WH) plots [64–66]. The WH plots provide useful information regarding the effective particle size and lattice constant distribution based on the following equation:

$$\text{FWHM} \times \cos \theta / \lambda = 4\varepsilon \times \sin \theta / \lambda + k/D. \quad (1)$$

Here, λ is the wavelength of the x-rays used; ε is the distribution of the interplane distance, $\Delta d/d$; k is the Scherrer constant; and D is the apparent crystallite size. If $\text{FWHM} \times \cos \theta / \lambda$ is plotted against $\sin \theta / \lambda$ for each diffraction peak (Fig. 5), the effects of the particle size and lattice constant distribution can be estimated from the y intercept and the slope of the WH plot, respectively. From the y intercept values and the Scherrer constant k , the crystallite size can be determined

when the peak broadening due to small crystallite size effects is large [67].

Figure 5(a) shows the WH plots of the $\text{Nd}_2\text{Fe}_{14}\text{B}$ phase in the isotropic and anisotropic bulk-sintered magnets and the powdered single crystal at 300 and 600 K as well as that for a standard Si sample, which was analyzed to determine the instrumental resolution of the experimental configuration used in this study [58]. The WH plots of the different samples as measured at 600 K and that of Si were only slightly different, indicating that the effects of the lattice strain and a small crystallite size on peak broadening were negligibly small and within the limits of the instrumental resolution. Further, the WH plot of the powdered single crystal at 300 K was similar to that at 600 K. In contrast, the slopes of the WH plots of the isotropic and anisotropic bulk-sintered magnets at 300 K were larger than those of the plots measured at 600 K; however, the y intercepts of the plots were almost the same. This means that the peak broadening observed at 300 K was related to the distribution of the lattice constants of the isotropic and anisotropic samples. The ε values of the isotropic and anisotropic samples at 105 and 300 K were determined from the WH plots using the corrected FWHM values, that is, the FWHM_{cor} values. These values were determined by subtracting the effects of the instrument-related broadening (i.e., $\text{FWHM}_{\text{inst}}$) from the observed broadening (i.e., FWHM_{obs}), as shown below [65,66]:

$$\text{FWHM}_{\text{cor}} = \sqrt{\text{FWHM}_{\text{obs}}^2 - \text{FWHM}_{\text{inst}}^2}. \quad (2)$$

The $\text{FWHM}_{\text{inst}}$ values were taken to be those estimated using the Si sample. The WH plots using corrected FWHM values are shown in Fig. S2 [40]. Small y intercepts of the sintered magnets are consistent with an average particle size of approximately 5 μm , similar to that of the Si powder, which had an average particle size of approximately 5 μm . The estimated ε values of the isotropic and anisotropic bulk-sintered magnets were 0.036% and 0.026% at 300 K, respectively, and 0.050% and 0.037% at 105 K, respectively. Further, the degree of the lattice constant distribution of the anisotropic bulk-sintered magnet was approximately 70% of that of the isotropic sample.

D. Effects of pulverization on the crystallographic properties of $\text{Nd}_2\text{Fe}_{14}\text{B}$ phase

As described above, we confirmed that the lattice constants of the $\text{Nd}_2\text{Fe}_{14}\text{B}$ phase in the isotropic and anisotropic bulk-sintered magnets differed from those of the phase in the powdered single crystal. One of the primary differences between the three samples was their textures. However, it was essential to confirm whether the observed differences in the lattice constants were related to variations in the composition of the $\text{Nd}_2\text{Fe}_{14}\text{B}$ phase in the samples owing to chemical impurities. Thus, to elucidate the effects of the different textures on the $\text{Nd}_2\text{Fe}_{14}\text{B}$ phase with the same composition, we compared the lattice constants and FWHM values of the diffraction peaks of the isotropic and anisotropic bulk-sintered magnets with those of their powdered counterparts.

Figure 3 shows the temperature dependence of the lattice constants of the $\text{Nd}_2\text{Fe}_{14}\text{B}$ phase in the bulk-sintered magnets,

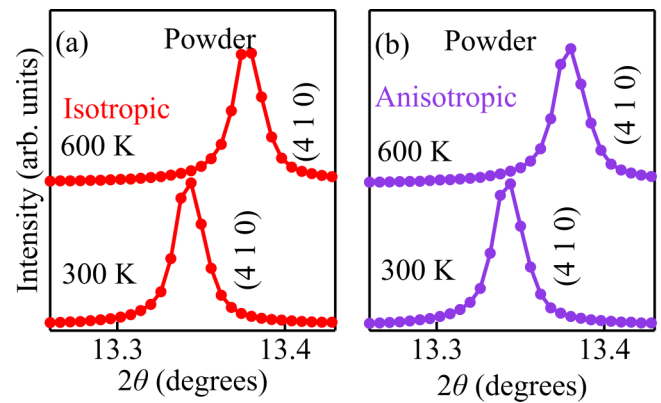


FIG. 6. Magnification of (4 1 0) peaks of the $\text{Nd}_2\text{Fe}_{14}\text{B}$ phase in powdered (a) isotropic and (b) anisotropic sintered magnets at 300 and 600 K.

their powdered counterparts, and the powdered single crystal. At temperatures higher than T_C , the lattice constants of the isotropic and anisotropic bulk-sintered magnets were similar to those of their powdered samples, whereas the values of a in the bulk and powdered sintered magnets were slightly smaller than that in the powdered single crystal. This difference is likely attributable to the small differences in the composition of the $\text{Nd}_2\text{Fe}_{14}\text{B}$ phase, with trace amounts of chemical impurities, such as Pr, in isotropic and anisotropic sintered magnets. To determine the exact reason for the difference, further studies are required on the $\text{Nd}_2\text{Fe}_{14}\text{B}$ lattice constants of various specimens, such as an uncrushed $\text{Nd}_2\text{Fe}_{14}\text{B}$ single crystal and crystal grains fabricated using different procedures. At temperatures below T_C , the a and c values of the powdered sintered magnets were larger and smaller, respectively, than those of the bulk-sintered magnets. This difference suggests that λ_a increased and λ_c decreased with the pulverization of the sintered magnets. As a result, the lattice constants in the powdered sintered magnets approached those of the powdered single crystal at temperatures lower than T_C .

The FWHM values of the diffraction peaks of the bulk-sintered magnets also changed with the pulverization. Figures 6(a) and 6(b) show the (4 1 0) diffraction peaks of the powdered samples as measured at 300 and 600 K. The FWHM values of the diffraction peaks of the powdered sintered magnets at 300 and 600 K were almost identical. However, they were slightly larger than those of the powdered single crystal; this was true even at 600 K. The observed broadening of the peaks was mostly attributable to the small crystal grain size after pulverization, as indicated by the larger y intercept in the WH plot [Fig. 5(b)]. Considering the y -intercept values and the Scherrer constant k of 0.89, the apparent crystallite size was estimated to be of submicron scale for both powdered samples. This is consistent with the SEM observation, in which small powder particles that are less than 0.5 μm in diameter were observed in the powdered sintered magnets. Parts of large particles observed in SEM images might consist of aggregates containing a few crystals. In contrast, the slopes of the WH plots of all the powdered samples at 300 K were smaller than those of bulk sintered magnets. These results suggest that the extent of peak broadening caused by the

distribution of the lattice constants was negligibly small for the powdered samples. Based on the above-described results, we can conclude that the observed differences in the lattice constants and FWHM values occurred because of the textural differences in the $\text{Nd}_2\text{Fe}_{14}\text{B}$ phase and not because of variations in its composition.

IV. DISCUSSION

A. Causes of differences in lattice constants of bulk-sintered magnets

We demonstrated that the lattice constants of the $\text{Nd}_2\text{Fe}_{14}\text{B}$ phase depend on the sample texture. To elucidate the underlying reason for this phenomenon, it was necessary to explain the variations in the lattice constants of the isotropic and anisotropic bulk-sintered magnets, their powdered counterparts, and the powdered single crystal at temperatures lower than T_C . In this section, we analyze this variability for bulk samples.

We have clarified that the difference in the lattice constants between samples originates from their anisotropic spontaneous magnetostrictive behavior. The estimated λ_a (λ_c) value is lower (higher) in bulk samples than in powdered samples. This means that the lattice expansion of the $\text{Nd}_2\text{Fe}_{14}\text{B}$ crystal grains along the a -axis (c -axis) associated with ferromagnetic ordering is lower (greater) in the bulk samples compared with that in the isolated crystal grains in the powdered samples. The crystallographic changes observed in the bulk specimens most likely originate from the internal compressive stress experienced by the individual $\text{Nd}_2\text{Fe}_{14}\text{B}$ crystal grains perpendicular to the c -axis. Because of the greater difference in the linear spontaneous magnetostriction values between isotropic bulk samples and powdered single crystals compared with that between anisotropic samples and powdered single crystals, the internal stress in an isotropic bulk sample should be greater than that in an anisotropic sample.

Given the distribution of lattice constants in the bulk samples as suggested by the observed broadening of the peaks (Sec. III C), it can be surmised that the internal stress is distributed throughout the magnets. The FWHM values of diffraction peaks of the isotropic bulk-sintered magnet were larger than those of the peaks of the anisotropic sample, indicating the stress distribution in the isotropic sample was wider. This would be in agreement with the previously reported presence of an internal stress in the secondary phases in bulk-sintered magnets [68]. It was found that the lattice constants of the secondary phases in bulk-sintered magnets were significantly greater than those of pristine metals and oxides as well as those of powdered sintered magnets [68].

To determine the origin of the internal stress in the bulk-sintered magnets, we considered the following two interactions that can generate internal stress: interactions between the $\text{Nd}_2\text{Fe}_{14}\text{B}$ and grain-boundary phases at their interface and interactions between neighboring $\text{Nd}_2\text{Fe}_{14}\text{B}$ grains. The former interactions originate from the difference in the extents of thermal expansion of the $\text{Nd}_2\text{Fe}_{14}\text{B}$ and grain-boundary phases, which can generate local stress at the interface. A few studies have reported that the structural mismatch between

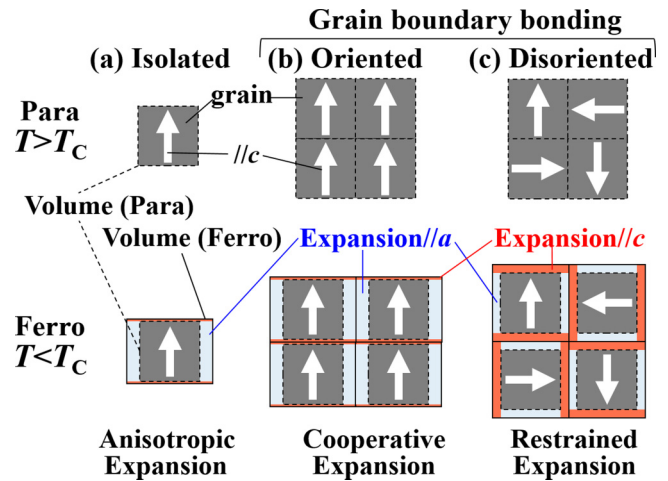


FIG. 7. Schematic of (a) an isolated $\text{Nd}_2\text{Fe}_{14}\text{B}$ crystal grain and (b) oriented and (c) disoriented grains with grain-boundary bonding in paramagnetic (Para, upper figures) and ferromagnetic (Ferro, lower figures) states. Arrows indicate the orientation of the c -axis of $\text{Nd}_2\text{Fe}_{14}\text{B}$ phase. Expansions along a -axis and c -axis associated with ferromagnetic ordering are represented in blue and red, respectively, in lower figures.

the $\text{Nd}_2\text{Fe}_{14}\text{B}$ and grain-boundary phases results in a local strain at their interface [45,69–72]. However, we believe that these interactions are not the primary cause of the internal stress, since high-angle annular dark-field scanning transmission electron microscopy performed using a thinned specimen has shown that the strain exists only in a limited area near the interface at a depth on the order of 10 nm [71,72]. In other words, the local lattice strain near the interface does not change the average lattice constant values of the $\text{Nd}_2\text{Fe}_{14}\text{B}$ phase.

Therefore, we attribute the internal stress to the interactions between the $\text{Nd}_2\text{Fe}_{14}\text{B}$ crystal grains in the bulk specimen caused by the large anisotropy arising from the thermal expansion of the $\text{Nd}_2\text{Fe}_{14}\text{B}$ phase at temperatures lower than T_C . To explain the relation between anisotropic spontaneous expansion and the arrangement of crystal grains, Fig. 7 illustrates the schematic of the arrangement of crystal grains for an isolated $\text{Nd}_2\text{Fe}_{14}\text{B}$ crystal grain, oriented grains with grain-boundary bonding (anisotropic sintered magnets), and disoriented grains with grain-boundary bonding (isotropic sintered magnets). The volume changes associated with linear spontaneous magnetostrictions along the a -axis and c -axis are denoted in blue and red, respectively. For the powdered sintered magnets, the estimated crystallite size was on submicron scale, which was smaller than that of one $\text{Nd}_2\text{Fe}_{14}\text{B}$ crystal grain in sintered magnets, as described above. The crystal grains in the powder samples as well as the single crystal are relaxed and do not experience interference from other grains [see Fig. 7(a)]. Thus, the internal stress is almost absent in these samples. In contrast, in the isotropic sintered magnets, the crystal grains were randomly oriented as confirmed by the magnetization measurement and synchrotron XRD profiles; further these grains were constructed with a grain boundary in the bulk specimen. Thus, the crystal grains in the isotropic bulk-sintered magnets are mutually stressed by the

anisotropic spontaneous magnetostriction that they experience [see Fig. 7(c)]. As a result, expansion along the a direction is constrained, resulting in an internal stress. Because of this internal stress along the a -axis direction, the length along the c -axis is longer compared with that for the isolated grains. In the anisotropic bulk-sintered magnets, the grains are aligned along the c direction [see Fig. 7(b)]. Thus, the lattice constants of the crystal grains vary almost simultaneously. However, the misalignment of the crystal grains can cause an internal stress. The presence of misalignment grains was confirmed by the FWHM of the rocking curves, as described above.

The spontaneous strain experienced by bulk materials is a general phenomenon observed in materials that exhibit significant anisotropic lattice deformation. Several rare-earth transition-metal permanent magnets, such as $\text{Sm}_2\text{Fe}_{17}$ and SmCo_5 magnets, also exhibit anisotropic spontaneous magnetostriction [51,73]. In addition to permanent magnets, negative-thermal-expansion materials with anisotropic structural changes have also been explored in recent years. It has been reported that the degrees of thermal expansion, determined through dilatometry measurements performed on bulk samples and XRD measurements on powder samples, differ significantly [74–76]. Understanding the origins of the strain produced in bulk materials by anisotropic structural changes is crucial for developing materials suitable for practical applications.

B. Influence of internal strain on magnetic properties

In the previous section, we discussed the internal stress induced in the bulk magnets by the large anisotropic thermal expansion of the $\text{Nd}_2\text{Fe}_{14}\text{B}$ phase at temperatures below T_C . It is natural to consider the inverse effect as well, namely, the internal stress affecting the magnetic properties of Nd-Fe-B magnets. In fact, when a pressure/strain is applied to ferromagnetic compounds, it often changes their magnetic properties [34,45,77–82]. For example, hydrostatic pressure changes the T_C value (−17.8 to −26.5 K/GPa) and the coercivity of the $\text{Nd}_2\text{Fe}_{14}\text{B}$ phase [34,79]. Theoretical and experimental studies have suggested the possibility that strain reduces coercivity [45,69,70,80]. For example, measurements performed using a Kerr microscope revealed that a uniaxial compressive stress of 0.1 GPa applied to anisotropic Nd-Fe-B sintered magnets induces a demagnetized area that is approximately 0.14% of the total area [81]. Moreover, a compressive pressure of approximately 0.18 GPa applied to $\text{Nd}_2\text{Fe}_{14}\text{B}$ reduces the coercivity by approximately 0.02 T [45].

Evaluation of the internal stress in bulk-sintered magnets can help one understand its effects on coercivity, although it is difficult to comment on its actual effects on the magnetic properties based only on the results of the present study. The internal stress experienced by the $\text{Nd}_2\text{Fe}_{14}\text{B}$ crystal grains can be estimated from the difference in the length along the a -axis of the grains in the bulk-sintered magnets and their powdered counterparts at 300 K; this difference is approximately 0.0052 Å for the isotropic sample and 0.0026 Å for the anisotropic sample. According to a previous report on the changes in the lattice constants under hydrostatic pressure, the c and a values at 300 K decrease linearly with increasing pressure ($da/dP = -0.0275$ Å/GPa and $dc/dP = -0.0343$ Å/GPa) [83]. Based

on this pressure dependence of the length along the a -axis, the internal pressure is estimated to be approximately 0.19 and 0.09 GPa for the isotropic and anisotropic bulk-sintered magnets, respectively. Using the elastic constant of $\text{Nd}_2\text{Fe}_{14}\text{B}$ perpendicular to the c -axis at 300 K (180 GPa) [82], the internal pressure along the a -axis is calculated to be approximately 0.1 and 0.05 GPa for the isotropic and anisotropic bulk-sintered magnets, respectively. Thus, the estimated internal pressures lie in the range of 0.05–0.19 GPa at 300 K, which corresponds to a decrease in the Curie temperature of approximately 1–5 K, assuming a hydrostatic applied pressure. Note that the actual change in the Curie temperature would be negligibly small, since the internal stress becomes very small at temperatures near T_C , as suggested by the negligibly small differences in the lattice constants of the sintered magnets and their powdered counterparts around T_C . However, the magnetic properties at 300 K could be affected by an increase in the internal pressure.

Next, we discuss the previously reported effects of the internal stress on the magnetic anisotropy energy, which is closely related to the coercivity. As per a previous study, these effects can be evaluated based on the lattice strain ε [80]. In the study, a 3% decrease in the lattice constant along the a -axis reduced the magnetocrystalline anisotropy from 5.1 to 1.4 MJ/m³. Thus, a 0.06% (0.03%) decrease in the a value of the isotropic (anisotropic) bulk-sintered magnet at 300 K would reduce magnetic anisotropy. However, the effect would be very small. From the above results, and focusing only on internal stress, the reduction of coercivity for isotropic bulk-sintered magnets seems to be larger than that for anisotropic samples, whereas the coercivity of the Nd-Fe-B sintered magnets is reported to decrease as the crystalline orientation of $\text{Nd}_2\text{Fe}_{14}\text{B}$ grains increases [55,56].

C. Using c/a ratio as indicator of internal strain

In this study, we showed that the lattice constants of the $\text{Nd}_2\text{Fe}_{14}\text{B}$ phase in polycrystalline specimens depend on the sample texture. To validate this conclusion, it was important to compare the lattice constant values obtained in this study with those reported in the literature [12–39]. However, the lattice constant values reported in the literature may contain systematic deviations related to the differences in the instruments and methods used. Thus, instead of evaluating the a and c values, we compared the c/a ratio because this value would be less sensitive to instrumental and experimental differences, such as origin shifts and differences in the wavelength. The lattice constants and c/a values are listed in Table S1 of the Supplemental Material [40].

Figure 8 shows the c/a values of the $\text{Nd}_2\text{Fe}_{14}\text{B}$ phase at room temperature classified by sample texture, i.e., powdered samples and single crystal, anisotropic bulk-sintered magnets, and isotropic bulk-sintered magnets. The isotropic bulk-sintered magnets exhibited the highest c/a values. Moreover, the c/a values of the anisotropic bulk-sintered magnets were larger than those of most of the single-crystal and powdered samples. The c/a values of the various Nd-Fe-B magnets could be grouped based on their texture. This result was in agreement with the expectation that the internal stress would be the highest in the isotropic sintered magnets, given

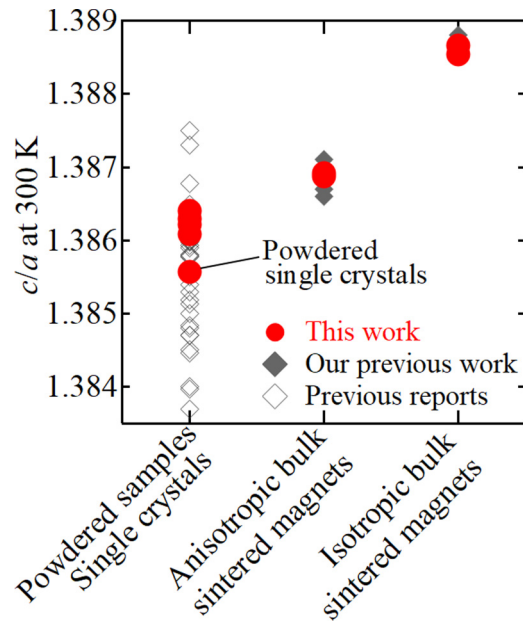


FIG. 8. Variations in c/a value of the $\text{Nd}_2\text{Fe}_{14}\text{B}$ phase at 300 K based on sample texture: powdered samples and single crystals, anisotropic bulk-sintered magnets, and isotropic bulk-sintered magnets [12–39].

that an internal compressive stress perpendicular to the c -axis would increase the c/a value. Thus, we expect that the c/a value scales with the internal stress and that it can be used as a reliable index of the internal stress to limit the effects of experimental errors.

Compared with the c/a values of the isotropic and anisotropic bulk-sintered magnets, those reported previously for powdered samples exhibited some variations. We believe that these variations can be ascribed to two other factors in addition to the experimental errors. The first factor is the differences in the chemical compositions of the $\text{Nd}_2\text{Fe}_{14}\text{B}$ phase because of chemical impurities, which changes the atomic distance and T_C , resulting in variations in the lattice constants at room temperature. The second factor is the internal stress experienced by the large polycrystalline particles in the powdered samples. Based on the origin of the internal stress in the isotropic sintered magnets, it is natural to assume that this stress remains in the large particles containing dozens of $\text{Nd}_2\text{Fe}_{14}\text{B}$ crystal grains. This can be confirmed by comparing the λ_c/λ_a value, which is closely related to the c/a value. Andreev *et al.* reported a λ_c/λ_a value of approximately 0.2 at 4.2 K using a single crystal [30]. This is similar to that obtained in the present study using the powdered single crystal ($\lambda_c/\lambda_a \simeq 0.2$ at 105 K). In contrast, Yang *et al.* reported a λ_c/λ_a value of approximately 0.6 at 10 K using pulverized melt-spun ribbons [27,44]. This is similar to the value obtained for the isotropic bulk-sintered magnets ($\lambda_c/\lambda_a \simeq 0.5$ at 105 K), suggesting that their specimens (melt-spun ribbons)

contained an internal stress because of their nanocrystalline isotropic structure. Moreover, their reported c/a value of 1.387 at room temperature was larger than those for the other pulverized samples but similar to those for the anisotropic bulk-sintered magnets.

The c/a data contain information about the internal stress experienced by the $\text{Nd}_2\text{Fe}_{14}\text{B}$ crystal grains. Similar variations in the lattice constants owing to the internal stress may be present in other materials as well, especially those with a large anisotropic thermal expansion coefficient. Thus, the c/a value may be used as an indicator of the internal stress in such materials.

V. SUMMARY

In this study, we systematically investigated the crystallographic properties of the $\text{Nd}_2\text{Fe}_{14}\text{B}$ phase using isotropic and anisotropic Nd-Fe-B bulk-sintered magnets, their powdered counterparts, and the powdered single crystal. Although the temperature dependence of the lattice constants of the $\text{Nd}_2\text{Fe}_{14}\text{B}$ phase was similar in all the investigated samples at temperatures higher than T_C , it differed significantly at temperatures lower than T_C . These results indicate that a compressive stress occurs perpendicular to the c -axis of the $\text{Nd}_2\text{Fe}_{14}\text{B}$ grains in the bulk-sintered magnets. This stress limits the spontaneous magnetostrictive expansion along the a -axis at temperatures below T_C . The internal stress on the $\text{Nd}_2\text{Fe}_{14}\text{B}$ grains can be attributed to the anisotropic volume changes of the surrounding $\text{Nd}_2\text{Fe}_{14}\text{B}$ crystal grains. Further, the internal stress in the isotropic bulk-sintered magnets is larger than that in the anisotropic bulk-sintered magnets. As a result, the c/a values of the $\text{Nd}_2\text{Fe}_{14}\text{B}$ phase in the Nd-Fe-B sintered magnets are larger than those of the phase in the powdered samples. Thus, it can be concluded that the presence of an internal stress in the polycrystalline specimens is one of the reasons for the variations in the values of the lattice constants reported in the literature.

ACKNOWLEDGMENTS

We thank T. Fukagawa and T. Nishiuchi of Hitachi Metals, Ltd. for providing the Nd-Fe-B sintered magnet samples and the results of magnetization measurements, and K. Sugimoto and M. Suzuki of the Japan Synchrotron Radiation Research Institute (JASRI) and M. Mito of the Kyushu Institute of Technology for valuable comments. This work was performed with the approval of the SPring-8 Program Advisory Committee (Proposals No. 2018A1009, No. 2018B1016, No. 2018B1333, and No. 2019A1007). This work was supported in part by the Elements Strategy Initiative Center for Magnetic Materials (ESICMM), (Grant No. JPMXP0112101004), which is funded by the Ministry of Education, Culture, Sports, Science and Technology (MEXT), Japan.

[1] J. F. Herbst, *Rev. Mod. Phys.* **63**, 819 (1991).
 [2] M. Sagawa, S. Fujimura, H. Yamamoto, Y. Matsuura, and K. Hiraga, *IEEE Trans. Magn.* **20**, 1584 (1984).

[3] M. V. Reimer, H. Y. Schenk-Mathes, M. F. Hoffmann, and T. Elwert, *Metals (Basel)* **8**, 867 (2018).

- [4] L. H. Lewis and F. Jiménez-Villacorta, *Metall. Mater. Trans. A* **44**, 2 (2013).
- [5] H. Nakamura, *Scr. Mater.* **154**, 273 (2018).
- [6] J. M. D. Coey, *Engineering* **6**, 119 (2020).
- [7] H. Sepehri-Amin, T. Ohkubo, T. Shima, and K. Hono, *Acta Mater.* **60**, 819 (2012).
- [8] K. Hono and H. Sepehri-Amin, *Scr. Mater.* **67**, 530 (2012).
- [9] K. Hirota, H. Nakamura, T. Minowa, and M. Honshima, *IEEE Trans. Magn.* **42**, 2909 (2006).
- [10] S. Hirosawa, *IEEE Trans. Magn.* **55**, 1 (2019).
- [11] H. Sepehri-Amin, T. Ohkubo, S. Nagashima, M. Yano, T. Shoji, A. Kato, T. Schrefl, and K. Hono, *Acta Mater.* **61**, 6622 (2013).
- [12] D. Givord, H. S. Li, and J. M. Moreau, *Solid State Commun.* **50**, 497 (1984).
- [13] C. B. Shoemaker, D. P. Shoemaker, and R. Fruchart, *Acta Crystallogr., Sect. C* **40**, 1665 (1984).
- [14] W. E. Wallace, F. Pourarian, A. T. Pedziwiatr, and E. B. Boltich, *J. Less Common Met.* **130**, 33 (1987).
- [15] M. Q. Huang, E. Oswald, E. Boltich, S. Hirosawa, W. E. Wallace, and E. Schwab, *Physica B+C (Amsterdam)* **130**, 319 (1985).
- [16] C. Hellwig and K. Girgis, *J. Alloys Compd.* **199**, 85 (1993).
- [17] G. K. Marasinghe, O. A. Pringle, G. J. Long, W. J. James, D. Xie, J. Li, W. B. Yelon, and F. Grandjean, *J. Appl. Phys.* **74**, 6798 (1993).
- [18] Y. Ying-chang, Z. Xiao-dong, K. Lin-shu, P. Qi, H. Yong-tian, H. Shuang, Y. Liu, and G. Sen-lin, *J. Less Common Met.* **170**, 37 (1991).
- [19] S. Sinnema, R. J. Radwanski, J. J. M. Franse, D. B. de Mooij, and K. H. J. Buschow, *J. Magn. Magn. Mater.* **44**, 333 (1984).
- [20] H. Oesterreicher, F. Spada, and C. Abache, *Mater. Res. Bull.* **19**, 1069 (1984).
- [21] R. Kamal and Y. Andersson, *Phys. Rev. B* **32**, 1756 (1985).
- [22] C. Abache and H. Oesterreicher, *J. Appl. Phys.* **60**, 1114 (1986).
- [23] P. l'Heritier, P. Chaudouet, R. Mader, A. Rouault, J.-P. Senateur, and R. Fruchart, *C. R. Acad. Sci. Paris* **299**, 849 (1984).
- [24] M. Abdul Matin, H.-W. Kwon, J.-G. Lee, and J.-H. Yu, *J. Magn.* **19**, 106 (2014).
- [25] Y. Li, M. Zhu, A. Li, H. Feng, S. Huang, W. Li, A. Di, and Y. Qi, *J. Rare Earths* **32**, 628 (2014).
- [26] M. A. Susner, B. S. Conner, B. I. Saparov, M. A. McGuire, E. J. Crumlin, G. M. Veith, H. Cao, K. V. Shanavas, D. S. Parker, B. C. Chakoumakos, and B. C. Sales, *J. Magn. Magn. Mater.* **434**, 1 (2017).
- [27] N. Yang, K. W. Dennis, R. W. McCallum, M. J. Kramer, Y. Zhang, and P. L. Lee, *J. Magn. Magn. Mater.* **295**, 65 (2005).
- [28] N. Tsuji, H. Okazaki, W. Ueno, Y. Kotani, D. Billington, A. Yasui, S. Kawaguchi, K. Sugimoto, K. Toyoki, T. Fukagawa, T. Nishiuchi, Y. Gohda, S. Hirosawa, K. Hono, and T. Nakamura, *Acta Mater.* **154**, 25 (2018).
- [29] H. Okazaki, D. Billington, N. Tsuji, W. Ueno, Y. Kotani, S. Kawaguchi, K. Sugimoto, K. Toyoki, T. Fukagawa, T. Nishiuchi, K. Hono, S. Hirosawa, and T. Nakamura, *Acta Mater.* **181**, 530 (2019).
- [30] A. V. Andreev, A. V. Deryagin, S. M. Zadvorkin, and S. V. Terent'ev, *Sov. Phys. Solid State* **27**, 987 (1985).
- [31] T. T. Sasaki, Y. Takada, H. Okazaki, T. Ohkubo, T. Nakamura, T. Sato, A. Kato, Y. Kaneko, and K. Hono, *J. Alloys Compd.* **790**, 750 (2019).
- [32] S. Obbade, P. Wolfers, D. Fruchart, R. Argoud, J. Muller, and E. Palacios, *J. Alloys Compd.* **242**, 80 (1996).
- [33] K. H. J. Buschow, D. B. De Mooij, J. L. C. Daams, and H. M. Van Noort, *J. Less Common Met.* **115**, 357 (1986).
- [34] M. Mito, H. Goto, K. Nagai, K. Tsuruta, H. Deguchi, T. Tajiri, and K. Konishi, *J. Appl. Phys.* **118**, 145901 (2015).
- [35] B. Rupp, A. Resnik, D. Shaltiel, and P. Rogl, *J. Mater. Sci.* **23**, 2133 (1988).
- [36] J. F. Herbst, J. J. Croat, and W. B. Yelon, *J. Appl. Phys.* **57**, 4086 (1985).
- [37] J. F. Herbst, J. J. Croat, F. E. Pinkerton, and W. B. Yelon, *Phys. Rev. B* **29**, 4176 (1984).
- [38] H. Boller and H. Oesterreicher, *J. Less Common Met.* **103**, L5 (1984).
- [39] O. Isnard, W. B. Yelon, S. Miraglia, and D. Fruchart, *J. Appl. Phys.* **78**, 1892 (1995).
- [40] See Supplemental Material at <http://link.aps.org/supplemental/10.1103/PhysRevMaterials.4.094405> for the room-temperature lattice constants in various reports, the temperature dependence of lattice constants of the Nd₂Fe₁₄B phase in isotropic and anisotropic sintered magnets and a powdered single crystal, SEM images, and the modified Williamson-Hall plots.
- [41] I. Poenaru, A. Lixandru, S. Riegg, B. Fayyazi, A. Taubel, K. Güth, R. Gauß, and O. Gutfleisch, *J. Magn. Magn. Mater.* **478**, 198 (2019).
- [42] Y. Matsuura, S. Hirosawa, H. Yamamoto, S. Fujimura, and M. Sagawa, *Appl. Phys. Lett.* **46**, 308 (1985).
- [43] H. Fujii, H. Nagata, Y. Uwatoko, T. Okamoto, H. Yamamoto, and M. Sagawa, *J. Magn. Magn. Mater.* **70**, 331 (1987).
- [44] N. Yang, K. W. Dennis, R. W. McCallum, M. J. Kramer, Y. Zhang, and P. L. Lee, *J. Appl. Phys.* **93**, 7990 (2003).
- [45] C. H. de Groot and K. de Kort, *J. Appl. Phys.* **85**, 8312 (1999).
- [46] D. Givord, H. S. Li, J. M. Moreau, and P. Tenaud, *J. Magn. Magn. Mater.* **54-57**, 445 (1986).
- [47] K. H. J. Buschow and R. Grössinger, *J. Less Common Met.* **135**, 39 (1987).
- [48] K. H. J. Buschow, *J. Less Common Met.* **118**, 349 (1986).
- [49] M. Shiga, *J. Phys. Soc. Jpn.* **50**, 2573 (1981).
- [50] E. F. Wassermann, *J. Magn. Magn. Mater.* **100**, 346 (1991).
- [51] K. H. J. Buschow, *Handbook of Magnetic Materials*, Vol. 8 (North Holland, 1995).
- [52] M. Shiga, *Curr. Opin. Solid State Mater. Sci.* **1**, 340 (1996).
- [53] A. Yasui, T. Nakamura, Y. Kotani, T. Fukagawa, T. Nishiuchi, and S. Hirosawa, *J. Appl. Phys.* **117**, 17B313 (2015).
- [54] W. F. Li, T. Ohkubo, and K. Hono, *Acta Mater.* **57**, 1337 (2009).
- [55] Y. Matsuura, J. Hoshijima, and R. Ishii, *J. Magn. Magn. Mater.* **336**, 88 (2013).
- [56] F. Cebollada, M. F. Rossignol, D. Givord, V. Villas-Boas, and J. M. González, *Phys. Rev. B* **52**, 13511 (1995).
- [57] S. Hirosawa, Y. Matsuura, H. Yamamoto, S. Fujimura, M. Sagawa, and H. Yamauchi, *J. Appl. Phys.* **59**, 873 (1986).
- [58] S. Kawaguchi, M. Takemoto, K. Osaka, E. Nishibori, C. Moriyoshi, Y. Kubota, Y. Kuroiwa, and K. Sugimoto, *Rev. Sci. Instrum.* **88**, 085111 (2017).
- [59] F. Izumi and K. Momma, *Solid State Phenom.* **130**, 15 (2007).
- [60] F. H. Spedding, J. J. Hanak, and A. H. Daane, *J. Less Common Met.* **3**, 110 (1961).
- [61] J. M. Leger, N. Yacoubi, and J. Loriers, *J. Solid State Chem.* **36**, 261 (1981).

- [62] J. Goutheron, D. Michel, A. M. Lejus, and J. Zarembowitch, *J. Solid State Chem.* **38**, 288 (1981).
- [63] D. Givord, J. M. Moreau, and P. Tenaud, *Solid State Commun.* **55**, 303 (1985).
- [64] G. K. Williamson and W. H. Hall, *Acta Metall.* **1**, 22 (1953).
- [65] Y. T. Prabhu, K. V. Rao, V. S. S. Kumar, and B. S. Kumari, *World J. Nano Sci. Eng.* **04**, 21 (2014).
- [66] K. Baroudi, B. D. Gaulin, S. H. Lapidus, J. Gaudet, and R. J. Cava, *Phys. Rev. B* **92**, 024110 (2015).
- [67] F. T. L. Muniz, M. A. R. Miranda, C. Morilla dos Santos, and J. M. Sasaki, *Acta Crystallogr. Sect. A Found. Adv.* **72**, 385 (2016).
- [68] S. Kobayashi, A. Martín-Cid, K. Toyoki, H. Okazaki, S. Hirose, and T. Nakamura, *AIP Adv.* **9**, 125154 (2019).
- [69] G. Hrkac, T. G. Woodcock, C. Freeman, A. Goncharov, J. Dean, T. Schrefl, and O. Gutfleisch, *Appl. Phys. Lett.* **97**, 232511 (2010).
- [70] G. Hrkac, T. G. Woodcock, K. T. Butler, L. Saharan, M. T. Bryan, T. Schrefl, and O. Gutfleisch, *Scr. Mater.* **70**, 35 (2014).
- [71] Y. Murakami, T. T. Sasaki, T. Ohkubo, and K. Hono, *Acta Mater.* **101**, 101 (2015).
- [72] T. T. Sasaki, T. Ohkubo, and K. Hono, *Acta Mater.* **115**, 269 (2016).
- [73] A. V. Andreev, F. R. de Boer, T. H. Jacobs, and K. H. J. Buschow, *Physica B Condens. Matter* **175**, 361 (1991).
- [74] K. Takenaka, Y. Okamoto, T. Shinoda, N. Katayama, and Y. Sakai, *Nat. Commun.* **8**, 14102 (2017).
- [75] N. Katayama, K. Otsuka, M. Mitamura, Y. Yokoyama, Y. Okamoto, and K. Takenaka, *Appl. Phys. Lett.* **113**, 181902 (2018).
- [76] N. Zhang, L. Li, M. Wu, Y. Li, D. Feng, C. Liu, Y. Mao, J. Guo, M. Chao, and E. Liang, *J. Eur. Ceram. Soc.* **36**, 2761 (2016).
- [77] L. Patrick, *Phys. Rev.* **93**, 384 (1954).
- [78] H. Nagata, S. Hirose, M. Sagawa, A. Ishibashi, and S. Endo, *J. Magn. Magn. Mater.* **70**, 334 (1987).
- [79] J. Kamarád, Z. Arnold, and J. Schneider, *J. Magn. Magn. Mater.* **67**, 29 (1987).
- [80] M. Yi, H. Zhang, O. Gutfleisch, and B.-X. Xu, *Phys. Rev. Appl.* **8**, 014011 (2017).
- [81] M. Takezawa, Y. Morimoto, J. Ejima, Y. Nakano, and T. Araki, *IEEE Trans. Fundam. Mater.* **137**, 367 (2017).
- [82] M. Shiga, Y. Kusakabe, Y. Nakamura, K. Makita, and M. Sagawa, *Physica B Condens. Matter* **161**, 206 (1990).
- [83] T. Tajiri and M. Mito, *J. Magn. Magn. Mater.* **498**, 166163 (2020).